Mean Flows and the Onset of Chaos in Large-Cell Convection

H. S. Greenside,[1] M. C. Cross,[2] and W. M. Coughran, Jr.[3]
[1]*Department of Computer Science and Department of Physics, Duke University, Durham, North Carolina 27706*
[2]*Division of Physics, Mathematics, and Astronomy, California Institute of Technology, Pasadena, California 91125*
[3]*Computing Mathematics Research Department, AT&T Bell Laboratories, Murray Hill, New Jersey 07974*
(Received 24 December 1987)

Numerical simulations of two-dimensional model equations show that a coupling between amplitude and vertical-vorticity fields allows chaotic flows near the onset of Rayleigh-Bénard convection in large-aspect-ratio domains. In cylindrical cells, mean flows arising from this coupling lead to a chaotic nucleation of dislocations that is remarkably similar to recent observations in convection experiments.

PACS numbers: 47.20.Bp, 47.20.Tg, 47.25.Ae

Recent optical studies of the transition to chaos in convecting fluids[1-3] have provided valuable insights on the pioneering experiment of Ahlers and Behringer.[4] The latter experiment, by the measurement of the time dependence of vertical heat transport through a convecting fluid, showed that chaotic states existed close to onset in large-aspect-ratio cells, a conclusion in naive contradiction with the existence of a finite band of linearly stable wave numbers.[5] The recent visual experiments confirmed that chaos can occur near onset, and that this chaos is associated with the dynamics of defects (disruptions of the local periodicity) in the convection rolls. In particular, a simple repetitive defect nucleaton mechanism was found close to onset[1] for fluids with Prandtl numbers $\sigma \simeq 0.7$.

In this Letter, we demonstrate that a key theoretical element for understanding these experimental results is the generation of mean flows, i.e., flows whose length scales are large compared to the wavelength of convection rolls. Mean flows arise when vertical vorticity is driven by roll curvature and amplitude modulations.[6] This coupling has been conjectured[6-8] to be important in understanding the transition to chaos for fluids with small to intermediate Prandtl numbers ($\sigma \lesssim 1$), and is a crucial ingredient in a correct description of long-wavelength instabilities such as the skewed varicose.[9] Mean flows have been observed experimentally but only for certain stationary states,[10] e.g., nearly axisymmetric rolls. We show here for the first time that such a coupling actually leads to chaotic, yet experimentally reasonable, flows.

This conclusion is especially interesting since it is known that time-dependent states can arise quite generally from the competition of different wavelength selection mechanisms.[11] These mechanisms occur in the presence of finite lateral walls or of different kinds of defects such as focus singularities or grain boundaries. By numerical simulation of model equations in large domains, we have found that evolutions governed solely by competition between wavelength selection mechanisms [e.g., Eqs. (1)-(4) below with $g=0$] are asymptotically periodic or stationary in time. Mean flows therefore play a major role in the generation of chaos near onset.

Our results are obtained by numerical integration of 2D model equations of convection. These equations generalize the Swift-Hohenberg equation,[12] which has been shown by analytical[8] and numerical[13] studies to reproduce complex pattern formation of convecting fluids near onset. The equations we use are the following:

$$(\partial_t + \mathbf{U}\cdot\nabla)\psi(x,y,t) = \left[r - (\Delta+1)^2\right]\psi + \psi^2\Delta\psi, \quad (1)$$

$$\Delta^2\zeta(x,y,t) = g\nabla\psi\times\nabla\Delta\psi\cdot\hat{\mathbf{z}}, \quad (2)$$

$$\mathbf{U}(x,y,t) = \nabla\times(\zeta\hat{\mathbf{z}}), \quad (3)$$

with boundary conditions

$$\psi = \mathbf{n}\cdot\nabla\psi = 0, \quad \zeta = n\cdot\nabla\zeta = 0, \quad (4)$$

where $\mathbf{n}$ is a vector normal to the boundaries, and the operator $\nabla = \partial_{xx}^2 + \partial_{yy}^2$ is the 2D Laplacian.

The fields and parameters in Eqs. (1)-(4) have the following meanings. The field $\psi(x,y,t)$ can be considered proportional to the fluid temperature in the midplane of a convection cell. (The midplane is described by Cartesian coordinates x and y which have been normalized to the depth of the fluid; the direction of gravity is $-\hat{\mathbf{z}}$; the time is measured in units of the vertical thermal diffusion time t_v.) The field $\zeta(x,y,t)$ is a vorticity potential, with $-\Delta\zeta = \Omega\cdot\hat{\mathbf{z}}$ giving the vertical component of vorticity $\Omega = \nabla\times\mathbf{U}$. The variable r in Eq. (1) is an effective Rayleigh number or bifurcation parameter, measuring the extent to which the convecting fluid is driven out of equilibrium by a vertical temperature gradient. For laterally infinite cells, $\psi = 0$ is the only stable state for $r < 0$. The parameter g in Eq. (2) is some measure of the Prandtl number σ, with large g corresponding to small σ. Another parameter enters for finite cells: The aspect ratio Γ is a typical lateral dimension normalized to half the critical wavelength $\lambda_c/2 = \pi/k_c$, where k_c has been set equal to 1 in Eq. (1).

These equations, although much simpler than the five Boussinesq equations in three space dimensions, still contain the basic physics of convection near onset: a continuous transition to a spatially periodic state as some

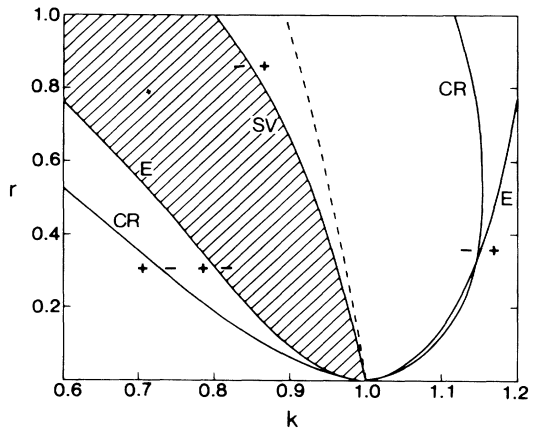

FIG. 1. Stability diagram for 1D rolls of wave number k for Eqs. (1)–(4) when $g=10$. The various lines are stability boundaries for CR, Eckhaus (E), and SV instabilities. The + and − signs indicate the sign of the eigenvalue upon crossing of a boundary; the region of stable wave numbers is shaded. The dotted line is the selected wave number for axisymmetric rolls.

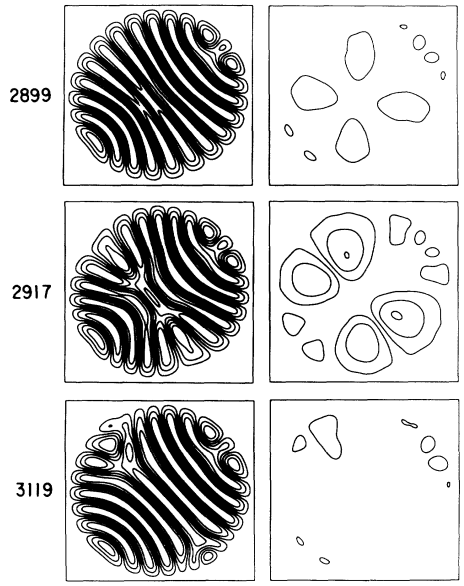

FIG. 2. Contour plots of the amplitude field $\psi(x,y,t)$ (left panels) and the vertical vorticity potential $\zeta(x,y,t)$ (right panels) at times $t=2899$, 2917, and 3119, from a numerical simulation of Eqs. (1)–(4) for $\Gamma=7$, $r=0.5$, and $g=10$.

physical parameter (here r) is increased; stable states whose wave numbers are limited by linear instabilitites such as the Eckhaus, crossroll (CR), zigzag, and skewed varicose (SV)[5,14] as shown in Fig. 1; boundary conditions [Eq. (4)] that force nontrivial constraints on convection rolls, e.g., that rolls are normal to boundaries; and a coupling to vertical vorticity that leads to mean flows.

The nonlinear term $\psi^2\Delta\psi$ in Eq. (1) and the operator on the left side of Eq. (2) are particular choices from the class of models considered previously.[14] The original motivation was to construct models for which the wave number selected by axisymmetric convection (the dashed line in Fig. 1) lay outside the stable band,[8] and was also unstable to the SV instability at higher Rayleigh number. Although the states we study are typically not axisymmetric, other models that we have investigated for which this criterion was not satisfied[14] do not show chaos. The vorticity equation, Eq. (2), corresponds to the suggestion of Siggia and Zippelius[6] for free-slip convection, except for the absence of a time derivative on the left side, which eliminates the oscillatory instability. We consider this a useful simplification in interpreting time-dependent flows near threshold.

Efficient numerical codes for solving these model equations have been developed in cylindrical,[15] rectangular,[13] and periodic[13] geometries. The simplicity of these equations allows long integrations (many horizontal diffusion times $\tau_h \approx \Gamma^2$) in large cells ($\Gamma \lesssim 30$), permitting a detailed study of the pattern evolution and a statistical analysis of corresponding time series. Typical runs involved our fixing the parameters r, g, and Γ, specifying an initial condition $\psi_0=\psi(x,y,0)$, and integrating for a time $t \lesssim 50\tau_h$. Initial conditions consisted of random fields, 1D rolls of given wave number k, or the final state of a previous integration which possibly had different parameter values. Only small portions of the 4D parameter space $\langle r,g,\Gamma,\psi_0\rangle$ have been explored.

Our main result is the discovery of chaos in cylindrical cells over a range in r for $g=10$, and the similarity of the evolving spatial patterns to recent optical experiments. Representative spatial evolutions of chaotic states are given in Figs. 2 and 3. Both close to onset in large cells and further from onset in smaller cells, the chaotic dynamics are similar to that first described by

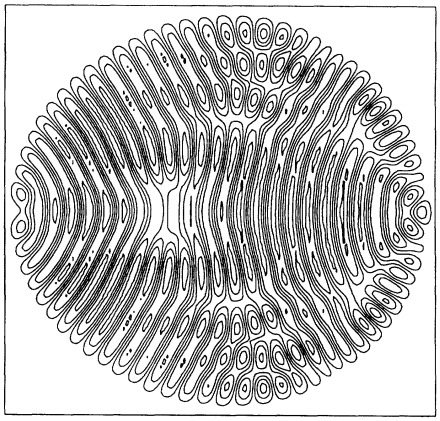

FIG. 3. Contour plot of $\psi(x,y,t)$ at time $t=818$, close to onset ($r=0.08$), and for a large aspect ratio ($\Gamma=14$).

Pocheau, Croquette, and Le Gal[1]: compression of rolls centered on focus singularities, nucleation of two dislocations, and climbing of these defects towards the lateral walls, where they annihilate. The process repeats itself irregularly. For the $\Gamma=7$ cell, the dislocations disappear directly at the lateral wall, while for the $\Gamma=14$ cell, the dislocations climb towards the wall, then glide towards the focus singularity where they disappear. The latter case is seen experimentally.[1]

The contour plots of the vorticity potential in Fig. 2 are the stream lines of the mean flows U in the convecting fluid. Four regions of vertical vorticity build up, with the corresponding mean flows advecting fluid towards the center of the cell. This compresses the central rolls until two dislocations nucleate, at which point vorticity dipoles appear centered on the defects. Measurements of local wave numbers show that the mean flows decrease wave numbers near the lateral wall and increase wave numbers near the center of the cell. The central wave number increases rapidly with time until it lies significantly beyond the SV boundary, approaching closely to the Eckhaus and CR boundaries before defects appear (Fig. 4). As the dislocations appear, the ζ field decreases rapidly in magnitude, and the local wave numbers are restored to values close to k_c, so that they lie within the stability band (Fig. 4). A symmetry breaking occurs in which defect nucleation alternates successively on either side of the vertical symmetry line, which also agrees with experiment.[1] At much later times, the axis of symmetry might rotate through some finite angle as seen in Fig. 2.

The extreme values attained by the central wave number in Fig. 4 (well beyond the SV branch) are difficult to reconcile with the linear stability diagram, Fig. 1. One might guess that extreme wave numbers occur because compression of the rolls by mean flows is occurring faster than the growth of linear instabilities. This idea is contradicted by stable stationary states found near onset in slight smaller-aspect-ratio cells, for which the central wave number lies well beyond the SV boundary. This suggests that curvature of the rolls significantly alters the applicability of the linear stability analysis, stabilizing rolls with large wave numbers. This conclusion is in agreement with small-r laboratory experiments, which also found stationary states with local wave numbers that sit significantly outside the band of stable wave numbers.[1]

A representative chaotic times series and power spectrum for the mean square amplitude $\langle\psi^2\rangle$ (which is linearly related to the vertical heat transport) are given in Fig. 5 for $r=0.5$ and $\Gamma=7.0$. The time series is clearly chaotic out to the longest integration times of about $150\tau_h$, which implies that the series is statistically sta-

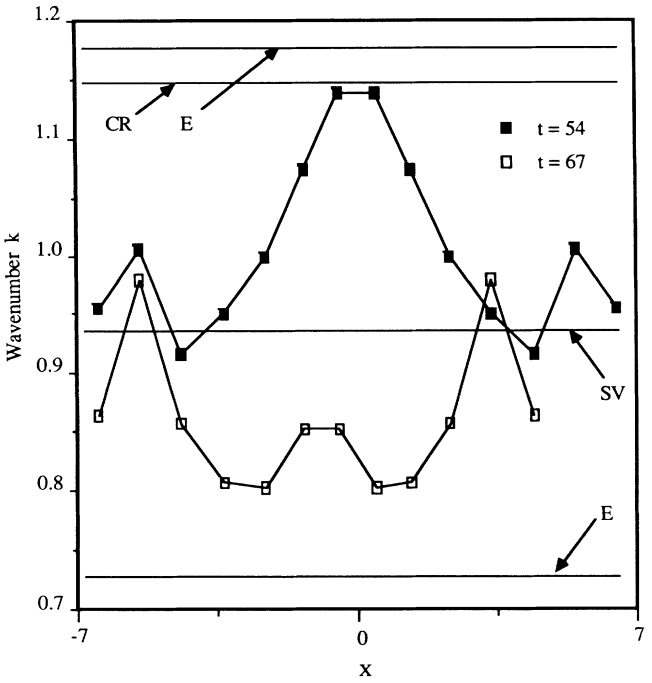

FIG. 4. Wave number distribution $k(x)$ across the center of the cell just above ($t=54$) and after ($t=67$) nucleation of two dislocations, for parameters $\Gamma=7$, $r=0.5$, and $g=10$. The lines denote where the Eckhaus, SV, and cross-roll stability boundaries lie, derived from Fig. 1.

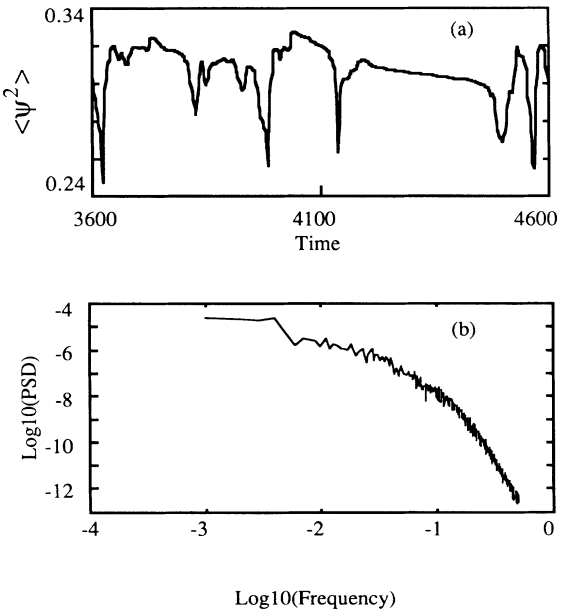

FIG. 5. (a) Time dependence of $\langle\psi^2\rangle$, for the chaotic run of Fig. 2, with $\Gamma=7$ and $r=0.5$. The short vertical-diffusion time scale of the nucleation events (widths of the sharp peaks) and the longer horizontal-diffusion time scale separating the peaks (representing wave-number adjustment) are in good agreement with experiment (Ref. 1). (b) Corresponding power spectrum.

tionary. Further evidence that the time series is chaotic comes from an estimate of its fractal dimension with a cluster algorithm,[16] which gives a surprisingly low value of 2.9 for a series of 4096 points. This dimension is greatly smaller than the phase-space dimension of ≈ 16000 representing the total number of numerical degrees of freedom used in the simulation. The power spectrum of $\langle\psi^2\rangle(t)$ in Fig. 5(b) is broad band, roughly constant at low frequencies and falling off approximately as a power law at higher frequencies, with an exponent of about -6. This behavior is consistent with several experiments,[4] although experiments give a power closer to -4. This result also suggests that deterministic dynamics suffice to generate approximate power-law behavior in the spectral density at high frequencies.[17]

To study how the above results depend on the geometry of the domain, many of the above runs were repeated in rectangular cells [with the boundary conditions Eq. (4)] and in square periodic domains (for which boundary conditions are automatically satisfied by use of periodic representations for the fields). For $g=10$ and $r=0.5$, and for comparable aspect ratios, chaotic states were found in rectangular cells but not in periodic domains; in the latter case only time-independent states consisting of parallel or wavy rolls were attained asymptotically. The existence of chaotic states near onset in rectangular domains is in qualitative agreement with recent cryogenic experiments;[18] our simulations predict that the spatial chaos involves two or more focal singularities at corners that evolve in a complicated way that will be described elsewhere. The absence of chaos in periodic domains ($\Gamma=10$ and $\Gamma=14$ for $r=0.5$ and $g=10$) was unexpected, and suggests that lateral walls play a crucial role in driving mean flows that lead to defect nulceation and chaos.

The above simulations in cylindrical cells are in agreement with experiments on fluids with $\sigma \leq 0.7$ (see Ref. 1 and Gao and co-workers[19]), but do not agree with slightly higher Prandtl number experiments,[2,3] in which a transition to chaos was seen very close to the onset of convection. The latter experiments involved the dynamics of grain boundaries near the lateral walls, with some local wave numbers being unstable to the zigzag instability.[3] Our simulations for both rectangular and cylindrical geometries show that there are no time-dependent states for $r_c < r < r_1$ where $r_c(\Gamma)$ is the critical value for onset in a domain of finite aspect ratio Γ, and where $r_s(\Gamma)$ is a decreasing function of aspect ratio and also depends on the cell geometry; we estimate $r_1(7) \approx 0.1$ and $r_1(14) \approx 0.03$ for cylindrical cells. The absence of chaotic states very close to onset in our model equations is not understood, but a possible explanation is that the vorticity coupling in Eqs. (1)–(3) leads to a zig-zag instability that is no longer a long-wavelength instability, as it is for the Boussinesq equations with nonslip boundary conditions.[6]

In summary, we have numerically studied the behavior of model equations that describe the onset of chaos in large-aspect-ratio convection. These simulations show that mean flows driven by distortions of the rolls can produce chaotic states in cylindrical cells that are remarkably similar to recent experiments on fluids with Prandtl number 0.7.

We would like to thank Guenter Ahlers, Bill Baxter, Robert Behringer, Petter Bjørstad, Jerry Gollub, Michael Heutmaker, and Pierre Hohenberg for useful discussions. This work was supported by a United States Department of Energy Grant No. DE-AC02-76-CHO-3073, by an Office of Naval Research Grant No. N00014-85-K-0487, by a National Science Foundation Grant No. DMR-8412543, and by computer time made available at the San Diego Supercomputer Center.

[1]A. Pocheau, V. Croquette, and P. Le Gal. Phys. Rev. Lett. **55**, 1094 (1985); A. Pocheau, Ph.D. thesis, Université Pierre et Marie Curie, 1987 (unpublished).

[2]G. Ahlers, D. S. Cannell, and V. Steinberg, Phys. Rev. Lett. **54**, 1373 (1985).

[3]M. S. Heutmaker and J. P. Gollub, Phys. Rev. A **35**, 242 (1987).

[4]G. Ahlers and R. P. Behringer, Phys. Rev. Lett. **40**, 712 (1978); G. Ahlers and R. P. Behringer, Prog. Theor. Phys. Suppl. **64**, 186 (1978).

[5]F. H. Busse, Rep. Prog. Phys. **41**, 1829 (1978).

[6]E. D. Siggia and A. Zippelius, Phys. Rev. Lett. **47**, 835 (1981); A. Zippelius and E. D. Siggia, Phys. Rev. A **26**, 178 (1982).

[7]P. Manneville, J. Phys. (Paris), Lett. **44**, L903 (1983).

[8]M. C. Cross and A. C. Newell, Physica (Amsterdam) **10D**, 239 (1984).

[9]M. C. Cross, Phys. Rev. A **27**, 490 (1983).

[10]V. Croquette, P. Le Gal, A. Pocheau, and R. Guglielmetti, Europhys. Lett. **1**, 393 (1986).

[11]M. C. Cross, G. Tesauro, and H. S. Greenside, Physica (Amsterdam) **23D**, 12 (1986).

[12]J. Swift and P. C. Hohenberg, Phys. Rev. A **15**, 319 (1977).

[13]H. S. Greenside and W. M. Coughran, Jr., Phys. Rev. A **30**, 398 (1984).

[14]H. S. Greenside and M. C. Cross, Phys. Rev. A **31**, 2492 (1985).

[15]H. S. Greenside, W. M. Coughran, Jr., and P. Bjørstad, to be published.

[16]Y. Termonia and Z. Alexandrowicz, Phys. Rev. Lett. **51**, 1265 (1983).

[17]H. S. Greenside, G. Ahlers, P. C. Hohenberg, and R. W. Walden, Physica (Amsterdam) **5D**, 322 (1982).

[18]R. W. Motsay, K. E. Anderson, and R. P. Behringer, J. Fluid Mech. (to be published).

[19]H. Gao and R. P. Behringer, Phys. Rev. A **30**, 2837 (1984); R. P. Behringer, H. Gao, and J. N. Shaumeyer, Phys. Rev. Lett. **50**, 1199 (1983).